Article:
Luo, Y, Du, X and Wen, D (2015) Novel design of central dual-receiver for solar power tower. Applied Thermal Engineering, 91. pp. 1071-1081. ISSN 1359-4311

https://doi.org/10.1016/j.applthermaleng.2015.08.074

Novel design of central receiver for solar power tower

Yan Luo[1,2], Xiaoze Du[2†], Dongsheng Wen[1†]

1 School of Chemical and Process Engineering, University of Leeds, Leeds, LS2 9JT

2 School of Energy, Power and Mechanical Engineering, North China Electric Power University, Beijing 102206, China.

Abstract

A novel dual-receiver with a surrounding solar field was proposed to improve the efficiency of solar power tower (SPT). The new design combined an external and a cavity receiver, corresponding to the boiling and superheating sections respectively, and provided a simple yet controllable heat flux distribution on both sections. A case study of a 11MW solar power plant was conducted. It was demonstrated that the present dual-receiver could produce superheat steam of 515ºC and 10.7MPa at the solar heat absorbing efficiency of 86.55%. By considering various heat losses, the surface heat flux, the surface temperature, as well as the heat transfer fluid distributiuon were obtained for the dual-receiver. A comparison with two external cylindrical receivers showed that the present design could improve the global thermal efficiency by 3.2%. Off-design performance of the dual-receiver was obtained, which indicated that the plant performance was affected significantly by the incident solar fluxes at different time of a day. The influence of heat transfer tube size suggested that an optimized tube diameter for the superheating section of the present dual-receiver should be used. .

Keywords: solar power tower, dual-receiver, heliostat field, heat loss

† Corresponding author. Email address: duxz@ncepu.edu.cn (X. Du); D.Wen@leeds.ac.uk (D. Wen)

Nomenclature

A	area, m^2
a	void fraction in cross-section
c	specific heat capacity, J/(kg·^oC)
d	tube diameter, m
G	mass flow rate, kg/m^2· s
g	Gravitational acceleration, m/s^2
H	enthalpy of heat transfer fluid, J/kg
h	heat transfer coefficient, W/ m^2 K
l	boiler receiver height, m
m	mass flow rate, kg/s
Nu	Nusselt number
Pr	Prandtl number
P	pressure, Pa
q	incident solar energy flux, W/ m^2
Q	incident solar energy, W
Re	Reynolds number
T	temperature, K
u	fluid velocity, m/s
x	steam quality

Greek symbols

α	tube wall absorptivity
β	volumetric thermal expansion coefficient
ε	tube wall emissivity
η	thermal efficiency, %

λ thermal conductivity, W/m·K

μ dynamic viscosity, N·s/m^2

ν kinematic viscosity, m^2/s

ρ density, kg/m^3

Subscripts

B boiling receiver

Conv convective heat loss

f heat transfer fluid of one phase

foc forced convection of heat transfer fluid in the tube

gr difference between saturated and superheating parameter

i inner tube

in incident

j surface j

k surface k

lh latent heat

nc natural convective heat loss

rad radiative heat loss

ref reflective heat loss

s superheating receiver

sat saturated state

sl saturated liquid parameters

sub subcooling liquid

sv saturated vapor parameters

w tube wall

1 Introduction

Concentrated solar power (CSP) technologies offer promising options for high efficiency solar energy applications. Of all CSP technologies available, the solar power tower (SPT) can achieve higher temperatures up to 1000ºC and hence higher efficiency than that of parabolic trough and linear Fresnel systems [1]. SPT also has the greatest potential for cost reduction and efficiency improvement among all CSP technologies [1].

Most established solar tower power plants use water as heat transfer fluid (HTF), which is a mature and cost-effective configuration without extra energy storage [2]. For example, SUNSHING, Solar One, SPP-5, Beijing Badaling, PS10, PS20 and Sierra were direct steam generation solar thermal plants [1, 3-6], among which, SUNSHING, SPP-5, PS10 and PS20 were based on saturated steam, and others used superheated steam [1, 7].

No matter which condition applies, a single receiver on the top of the solar tower is always used either in the form of external cylinder or internal cavity, which includes both boiling and superheating sections. It was suggested that for plants capacity of exceeding 50MW with 6 hours of energy storage, external receiver in combination with a surrounding field should be used, rather than the cavity configuration with a fixed opening [8]. This was mainly based on the consideration of heliostat field efficiency, as the cavity configuration requires heliostats much far away from the tower and hence more atmospheric attenuation loss. A surrounding field is more suitable for large capacity plants. However, the single receiver design can bring many inherent constrains. For instance, as there is no saturated steam produced at the beginning of the start-up, it is easy to produce the overheating problem in the superheating section. This is why several solar tower power plants only used saturated steam as working fluid. In addition, the difference in the convective heat transfer coefficient of the two sections requires different allowable heat fluxes. It has been estimated that the maximum heat flux can be imposed on the boiling and superheating sections were

650kW/m^2 and 300kW/m^2, respectively [9]. Apparently it becomes difficult for the one-receiver configuration to control proper heat flux distribution on both sections.

Recently, some researchers have investigated the possibility of separating boiling and superheating sections. A patent was filed in 2011 that comprised two external cylinder receivers in series, one for boiling section and the other for superheating section [10]. Most recently, a patent proposed two cavities instead of external cylinders for the two sections [11]. In another configuration, an integrated receiver was designed that had a boiling section in tandem with a superheating section [12]. The receiver had a north-faced opening sector of 72º with the outer surface acting as the boiling section and the inner surface as the superheater. Because both inner and outer surfaces were heated, there was no suitable place for the downcomer, which was essential to ensure no vapor produced and hence avoiding the reduction in the fluid circulation velocity. The inner surface was served as a cavity receiver. However, the opening angle of 72º was so small that there was almost no incident flux distribution on side wall panels [12]. On the other hand, the inner surface had no cavity aperture inclination, which was necessary to reduce convective loss.

In order to avoid the problems presently existing, in this study a novel configuration of dual-receiver for solar tower power plant is proposed by combining the advantages both of the external and cavity receiver. In the new designed dual-receiver, the top is an external receiver to serve as the boiling section, and the bottom is a cavity one as the superheating section. The surrounding heliostat field is correspondingly divided into two parts, focusing lights onto the boiling and superheating sections, respectively. As a demonstration, the feasibility study of a 11MW solar tower power plant is conducted in this work, of which the configuration can be extended to larger capacity plants. It is expected that such a new idea would improve the efficiencies of solar towers by getting away from the drawbacks of the single receiver and fully utilizing its merits.

2 Physical model of the dual-receiver and its heliostat field

The configuration of the proposed dual-receiver with the schematic surrounding heliostat field is shown in Fig. 1. Taking water as heat transfer fluid, the top external receiver served as the boiling section for the solar power plant with a surrounding heliostat field, indicated as SF2 in Fig. 1. As the boiling temperature, ranged 300-400^{o}C, is relatively low, small convection and radiation heat losses are expected. The bottom cavity receiver serves as the superheating section, heated by north heliostat field SF1, shown in Fig. 1. Considering the high superheat temperature typically encountered, i.e., surface temperature ranges from 300^{o}C to 700^{o}C, a cavity structure is beneficial to reduce the convection and radiation losses. A steam drum is arranged on top of the external receiver, which is located at the height of 100.5m from the ground, similar to the arrangement of the PS10 power plant [13]. The cavity receiver center is located 13m blow the external receiver center.

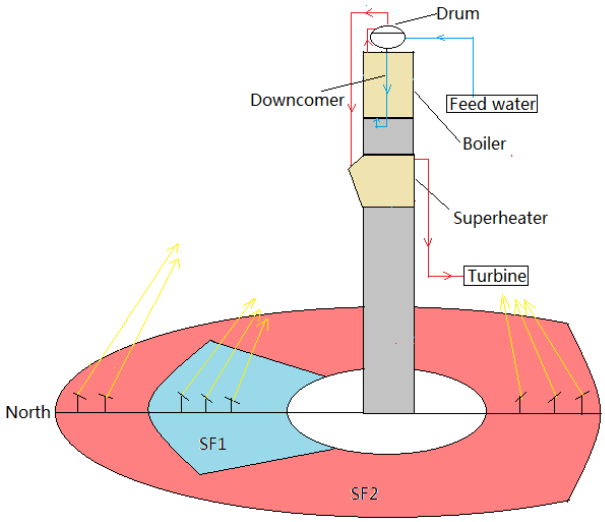

Fig. 1. Schematic diagram of the proposed dual-receiver with solar field.

A case study is conducted to illustrate the feasibility of the present concept. The heliostat field is designed to meet the requirement of a 11MW solar thermal power plant. The main parameters used in the optimization analysis are listed in Table 1.

Table 1. Main parameters used in the optical analysis.

Design parameters	
Latitude(^{o})	37.4
Time	Noon of the spring equinox day
DNI (W/m^2)	914
Design intercepted radiation (MW)	50
Solar multiple	1.33
Heliostats	
Count	624
Width (m)	12.84
Height (m)	9.45
Reflectivity	0.88
Optical error (mrad)	2.9
Sun shape error (mrad)	2.51

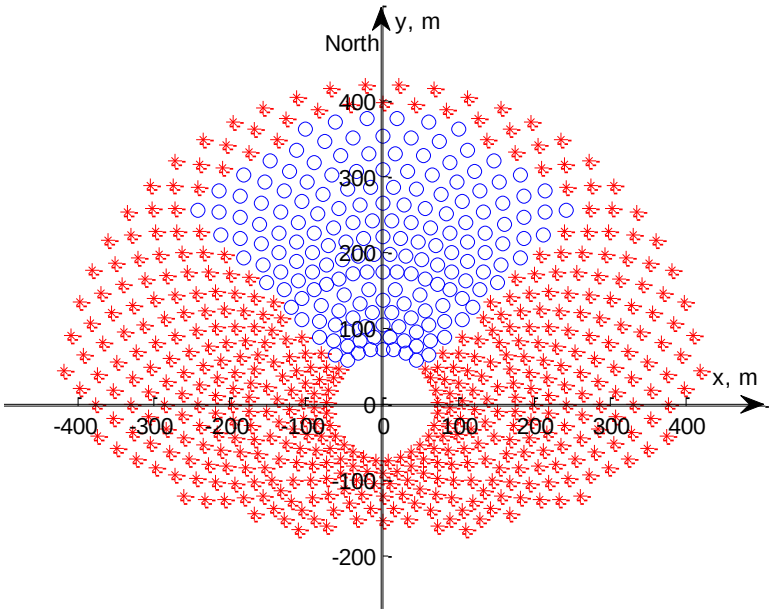

Fig. 2. Heliostat field layout of the proposed dual-receiver.

The heliostat field layout is optimized to obtain the maximum annual energy through the Campo code [14], which searches from the densest layout and then progresses towards expanded distributions. The resulted heliostat field layout divided into two sectors is shown in Fig. 2. The blue sector, which has a view angle of 90º and 182 heliostats, focuses the sunlight to the bottom superheater. The red sector has 442 heliostats and is dedicated to the top boiler section. The total efficiency of heliostat field obtained is 72.17%.

3 Thermal analysis of the dual-receiver

3.1 Dual-receiver geometry

To compare with a typical SPT system, the inlet feed water temperature is set to be 205ºC and the outlet parameters of the superheat steam are 10.7MPa and 515ºC, respectively.

The top external receiver has a cylindrical shape with height of 10m and diameter of 7m. The receiver comprises 16 parallel rising panels. The outer diameter of each tube is 26.7mm and wall thickness is 4mm. All tubes are made of SA-192 carbon steel with a yield strength of 180MPa and an allowable temperature of 510ºC [12]. The boiler is of a drum type with forced circulation and the outlet steam quality is 0.1.

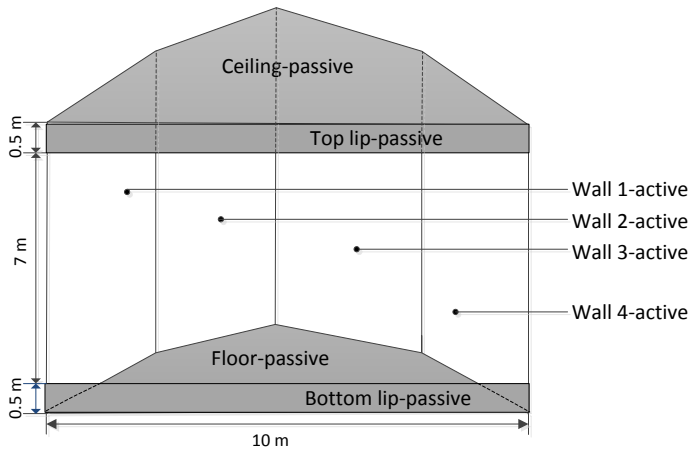

(a) The cavity receiver geometry.

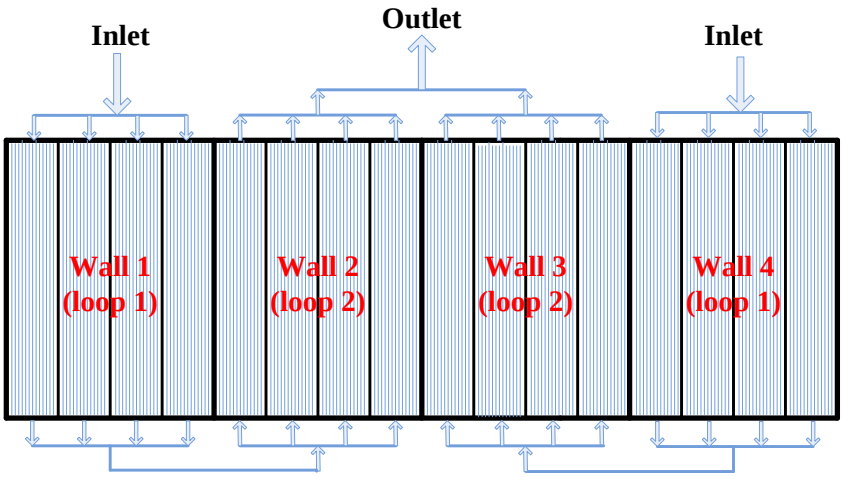

(b) Fluid flow layout of the active heated walls.

Fig. 3. The bottom cavity receiver.

The bottom cavity receiver has a half octagon shape with height of 8m and radius of 5m, as shown in Fig. 3(a). The receiver inclination is 25º and has a 7×10m rectangular aperture. Each active heated wall has 4 panels, of which the fluid flow layout is shown in Fig. 3(b). The outer diameter of tube is also 26.7mm with a wall thickness of 4mm. The tube material is stainless steel SA-213TP304H, which has a yield strength of 206MPa and allowable temperature of 760ºC [12].

All tubes are coated by Pyromark with an emissivity of 0.95. The cavity ceiling, floor and lip passive insulation walls are made of ceramic fibers, whose emissivity is 0.2.

3.2 Surface heat flux distribution

The surface heat flux distribution of the present dual-receiver was obtained by the Monte-Carlo method. A multiple aim points strategy, proposed by [12], was applied under the condition of the maximum heat fluxes on the boiling and superheating sections below 650kW/m^2 and 300kW/m^2, respectively. Fig. 4 shows the simulated heat flux distribution of the dual-receiver. It can be obtained that the external receiver collected about 35.48MW solar heat. The active walls in the

bottom cavity receiver collected 14.19MW solar heat, while the ceiling-passive wall and floor-passive wall obtained incident solar heat of 0.25MW and 0.04MW, respectively.

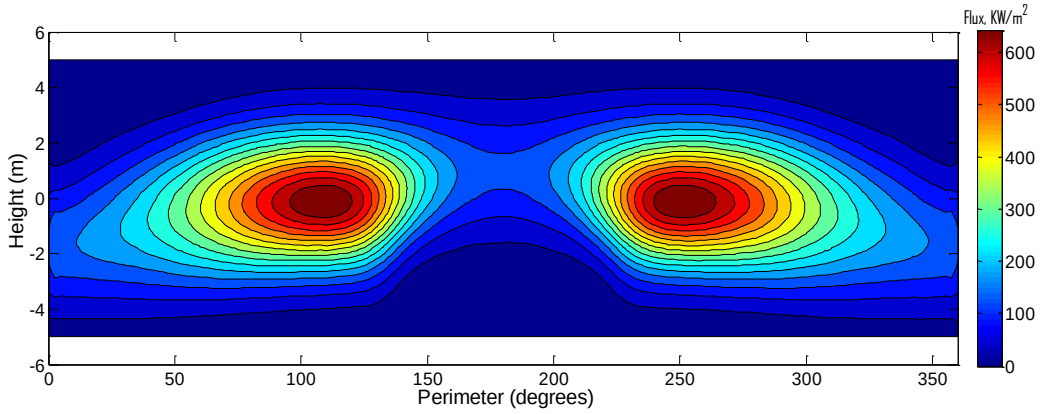

(a) Boiling receiver (Perimeter of 180 º is the north direction).

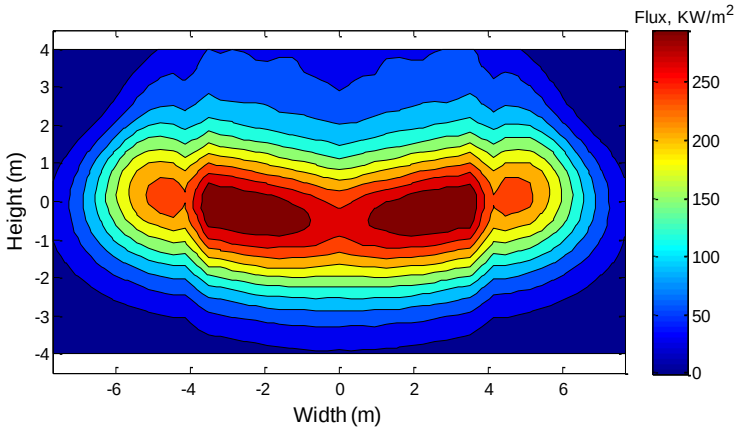

(b) Superheating receiver.

Fig. 4. Surface heat flux distribution for the dual-receiver at the noon of the spring equinox day.

3.3 Heat transfer analysis of the dual-receiver

3.3.1 Pressure drop

Considering the arrangement of the case study, the friction and gravity pressure drop dominates and the acceleration pressure drop can be neglected. The pressure drops of one-phase and two-phase flow were respectively calculated by [15],

$$-\frac{dp}{dz} = \pm\rho_f g + f\frac{\rho_f u^2}{2d_i} \quad (1)$$

$$-\frac{dp}{dz} = \pm(a\rho_{sv} + (1-a)\rho_{sl})g + \Phi^2 f_{sl} \frac{\rho_{sl} u^2 (1-x)^2}{2d_i} \tag{2}$$

where f is the friction factor, determined by the Moody's correlation [12], $\Phi^2 = 1 + 20/X_{tt} + 1/X_{tt}^2$, and X_{tt} is the Martinelli parameter.

3.3.2 Heat transfer coefficient

For single phase water only or vapor only flowing in the tube, the heat transfer coefficient can be obtained by the Dittus-Boelter's equation [16],

$$h_f = 0.023\lambda_f \, Re_f^{0.8} \, Pr_f^{0.4} / d_i \tag{3}$$

Totally three subcooled boiling regimes can be distinguished in the heated panels of the top cylinder receiver, namely partial flow boiling, fully developed boiling and significant void flow. The onset point of the subcooled boiling was determined by the Bergles's equation [16],

$$T_w - T_{sat} = 0.556\left(\frac{q}{1082(10^5 P)^{1.156}}\right)^{0.463(10^5 P)^{0.0234}} \tag{4}$$

and the corresponding heat transfer coefficient of partial flow boiling was obtained by Moles and Shaw's formula [17],

$$h_{foc} = 78.5 h_f \, Bo^{0.67} \, Ja^{*-0.5} \, (\rho_{sv}/\rho_{sl})^{-0.03} \, Pr_f^{0.45} \tag{5}$$

where Bo is boiling number, $Bo = \frac{q}{GH_{lh}}$, and Ja^* is the Jakob number, $Ja^* = \frac{c(T_{sat} - T_f)}{H_{lh}}$.

Shah [17] obtained the onset superheat of the fully developed boiling as,

$$\frac{T_{sat} - T_f}{T_w - T_{sat}} = 2 \tag{6}$$

and the heat transfer coefficient for fully developed boiling and significant void flow, h_{foc}, can be calculated as [15],

$$h_{foc} = h_f (1/\ f(Bo) + x/x^*)^{-1} \tag{7}$$

where $f(Bo) = \begin{cases} 230Bo^{0.5}, Bo > 3\times10^{-5} \\ 1+46Bo^{0.5}, Bo \le 3\times10^{-5} \end{cases}$, $x = -\Delta T_{sub} c_f / H_{lh}$ and $x^* = -qc_f / (h_f H_{lh})$.

For the saturated boiling regime, Chen's formula [16] including the contributions from both macroscopic and microcosmic convection heat transfer was used ,

$$h_{foc} = h_{foc,mac} + h_{foc,mic} \tag{8}$$

$$h_{foc,mac} = 0.023\lambda_{sl}\, Re_{sl}^{0.8}\, Pr_{sl}^{0.4}\, K / d_i \tag{9}$$

$$h_{foc,mic} = 0.00122\left(\frac{\lambda_{sl}^{0.79} c_{sl}^{0.45} \rho_{sl}^{0.49}}{\sigma^{0.5} \mu_{sl}^{0.29} H_{lh}^{0.24} \rho_{sv}^{0.24}}\right)\Delta T_{gr}^{0.24} \Delta P_{gr}^{0.75} S \tag{10}$$

where K and S are empirical values, and σ is the surface tension.

3.3.3 Heat loss

The heat loss of the dual-receiver includes three parts, including that of reflective loss, radiative loss and convective loss. The conductive loss is very small and can be neglected in the analysis.

The heat loss for the top cylinder receiver for boiling can be obtained by the known tube wall temperature as follows [18],

$$Q_{B,ref} = A_B \cdot (1-\alpha) \cdot q_{B,in} \tag{11}$$

$$Q_{B,rad} = A_B \cdot \sigma \cdot \varepsilon \cdot (T_{B,w}^4 - T_\infty^4) \tag{12}$$

$$Q_{B,conv} = A_B \cdot h_{B,nc} \cdot (T_{B,w} - T_\infty) \tag{13}$$

in which, $h_{B,nc}$ can be acquired from $Nu_{B,nc} = \frac{h_{B,nc} l}{\lambda}$,

$$Nu_{B,nc} = (\frac{\pi}{2})0.098Gr^{1/3}(\frac{T_{B,w}}{T_\infty})^{-0.14} \quad (14)$$

in which, σ is the Boltzmann constant and $Gr = \frac{g\beta(T_{B,w} - T_\infty)l^3}{\nu^2}$ is the Grashof number.

Regarding the bottom receiver for superheating, eight sub-surfaces are considered including the aperture. The radiative heat loss is obtained by [19],

$$J_{S,rad,k} = \varepsilon_k \cdot \sigma \cdot T_{S,w,k}^4 + (1-\varepsilon_k)\sum_{j=1}^{8} F_{k,j} J_{S,rad,j} \quad (k = 1, 2, \ldots\ldots 8) \quad (15)$$

$$Q_{S,rad} = \sum_{k=1}^{7} A_{S,k} \cdot J_{S,rad,k} \cdot F_{k,8} \quad (16)$$

where $J_{S,rad,k}$ is the effective radiation leaving a surface including reflected fraction of the irradiation and direct emission. $F_{k,j}$ is the view factor between any two surfaces and evaluated by Nicolas Lauzier [20].

The reflective heat loss can be calculated similar to the radiative heat loss,

$$J_{S,ref,k} = (1-\alpha_k) \cdot q_{S,in,k} + (1-\alpha_k)\sum_{j=1}^{8} F_{k,j} J_{S,ref,j} \quad (k = 1, 2, \ldots\ldots 8) \quad (17)$$

$$Q_{S,ref} = \sum_{k=1}^{7} A_{S,k} \cdot J_{S,ref,k} \cdot F_{k,8} \quad (18)$$

where $J_{S,ref,k}$ is the effective reflection leaving a surface including re-reflected fraction and direct reflection for the incident solar energy.

The natural convective loss was based on the Siebers and Kraabel equation [18],

$$Q_{S,conv,k} = A_{S,k} \cdot h_{S,nc} \cdot (T_{S,w,k} - T_\infty) \quad (k = 1, 2, \ldots\ldots 7) \quad (19)$$

$$h_{S,nc} = 0.81(T_{S,w,average} - T_{\infty})^{0.426}(\frac{A_1}{A_2})(\frac{A_3}{A_1})^{0.63} \quad (20)$$

where $T_{S,w,average}$ is the average temperature of the active and passive heated surfaces, A_1 is the total interior cavity surface area, A_2 is interior cavity surface area below the horizontal plane, which cuts through the cavity at the top lip of the aperture, and A_3 is the difference between A_1 and the area of the bottom lip.

4 Results and discussions

4.1 Performance of the dual-receiver at the design conditions

The performance of the proposed dual-receiver was examined at the noon of the spring equinox day. For the top boiling receiver, the mass flow rate in each parallel rising panel was varied to ensure that the pressure drop through all panels was equal. Heat flux distribution was east-west symmetric, as shown in Fig. 4. For the east half of the boiling panels, from south to north, the average heat flux was 73.8kW/m^2, 108.4kW/m^2, 165.4kW/m^2, 234.1kW/m^2, 279.3kW/m^2, 247.4kW/m^2, 119.6kW/m^2 and 62.7kW/m^2, respectively. The corresponding mass flow rates to achieve the same pressure drop through all panels were acquired as 8.7kg/s, 11.1kg/s, 12.3kg/s, 11.9kg/s, 11.4kg/s, 11.8kg/s, 11.5kg/s and 7.6kg/s by Eq. (1)–(2). And the **inlet（boiler）** flow velocity of the panels varied from 0.8m/s to 3.6m/s

The surface temperature of the panel can be obtained by iteration. Firstly, the solar heat absorbing efficiency was assumed an initial value. The surface temperature of the panel was then obtained by considering the forced convection of the inner tube and the heat conductivity of the tube wall. Accordingly, new efficiency of each panel could be reached by calculating heat loss with the surface temperature distribution obtained. The iteration was terminated till a preset convergence criterion was reached, under which, the surface temperature distribution of the panel was acquired. Fig. 5 shows the resulted temperature distribution of the panel surface of the top boiling receiver.

The highest surface temperature was 398ºC, which was lower than the allowable temperature of 510ºC for SA-192 carbon steel. In the present design, the reflective, radiative and convective heat losses were calculated as 1774.1kW, 1554.1kW and 872.8kW, respectively, achieving a thermal efficiency of 88.16% for the top boiling receiver.

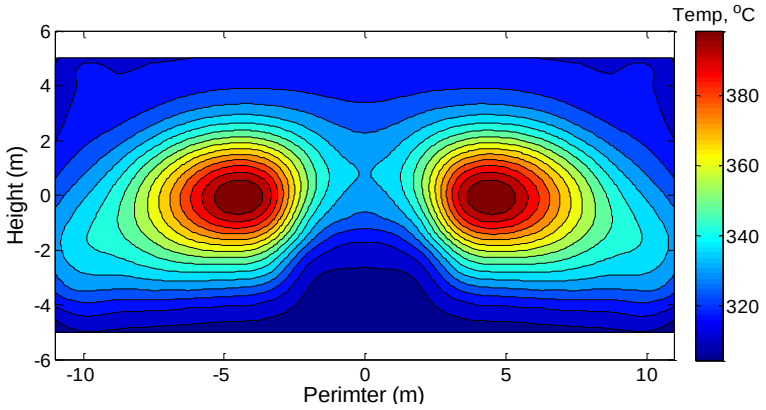

Fig. 5. Panel surface temperature distribution of the top boiling receiver (Perimeter of 0m is the north direction).

For the bottom superheating receiver, both east half and west half panels were split into two serial loops, as shown in Fig. 3. The mass flow rate of steam from the drum was 17.3kg/s, and was uniformly distributed at the inlets of the first loop. The outlets were mixed and fed into the second loop. The streamline velocity of superheat steam varied from 3.7 to 7m/s due to the change of steam density.

Similar iteration was executed to obtain the panel surface temperature distribution of the bottom cavity receiver, as shown in Fig. 6. The highest temperature was 733ºC, which also below the allowable temperature of 760ºC for SA-123TP203H. The total heat loss included reflective loss of 434.5kW, radiative loss of 1378.8kW and natural convective loss of 701kW, achieving a thermal efficiency of 82.64% for the superheating receiver.

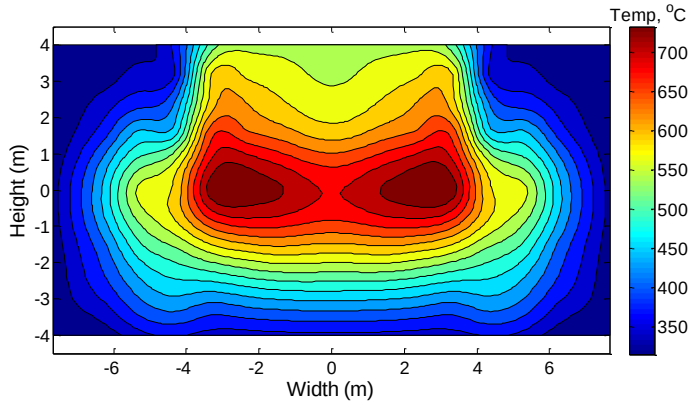

Fig. 6. Panels surface temperature distribution of the bottom superheating receiver.

4.2 Comparison of the present dual-receiver with a two-cylinder design under design conditions

To illustrate the advantages of the present new concept, a comparative study was conducted with a two-external cylindrical setup [10], as shown in Fig. 7. Both setups were based on a surrounding field and had two receivers, aiming for the separation of the boiling and superheating sections. Both setups were compared under the same conditions in terms as follows.

- design latitude and time;
- heliostat parameter, count and location;
- active heated surface area;
- receiver center height;
- inlet and outlet water/steam parameters.

The heliostat field layout of the two-external cylindrical setup is shown in Fig.8. The blue sector had 196 heliostats, which all focused sunlight onto the superheater, while the red sector for the boiler having 428 heliostats. The boiling receiver had a cylindrical shape with the height of 10m and the diameter of 7m. The superheating receiver was also cylindrical whose height and diameter were 8m and 4.87m, respectively.

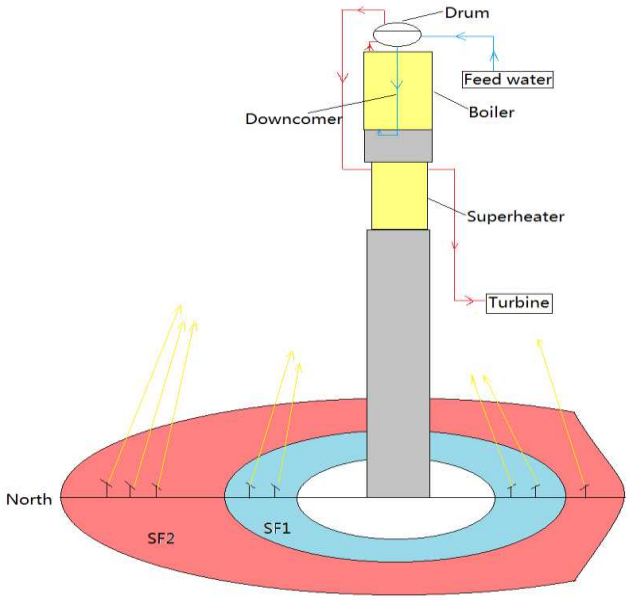

Fig. 7. Schematic diagram of the two-cylinder setup with surrounding heliostat field.

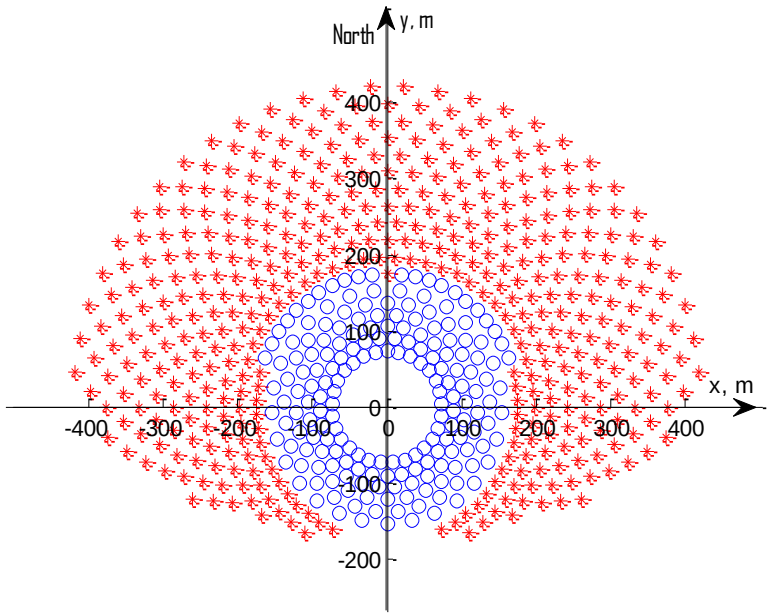

Fig. 8. Heliostat field layout of the two-cylinder setup.

For comparison, table 2 summarizes the geometry and thermodynamic parameters both of the present proposed dual-receiver and the two-cylinder setup.

Table 2. Geometry designs and thermodynamic parameters of the present dual-receiver and the two-cylinder setup.

	Geometry designs			Thermodynamic parameters of both designs	
		Present dual-receiver	Two-cylinder setup		
Boiling section	Center height (m)	100.5	100.5	Feed water temperature (^oC)	205
	Height (m)	10	10		
	Diameter (m)	7	7		
	Active heated surface area (m^2)	220	220		
	Tube outer diameter (mm)	26.7	26.7	Boiler outlet steam quality (%)	10
	Tube thickness (mm)	4	4		
	Number of panels (-)	16	16		
Superheating section	Center height (m)	87.5	87.5	Outlet superheating steam temperature (^oC)	515
	Height (m)	8	8		
	Diameter (m)	10	4.87		
	Aperture height (m)	7	-		
	Aperture width (m)	10	-		
	Active heated surface area (m^2)	122	122		
	Passive heated surface area (m^2)	95	-	Outlet superheating steam pressure (MPa)	10.7
	Tube outer diameter (mm)	26.7	26.7		
	Tube thickness (mm)	4	4		
	Number of panels (-)	16	16		

Table 3 gives solar field efficiency and thermal efficiency at the design conditions for the present proposed dual-receiver and the two-cylinder setup. To conduct a realistic comparisons, the inlet and outlet water/steam parameters of both receivers were set as the same as the Solar One plant with a known Rankine cycle efficiency of 35% [21]. As the same solar field and boiling receiver were

applied, the solar field efficiencies and the boiling receiver thermal efficiencies of both receivers were approximately similar.

However, the thermal efficiency of the bottom superheating receiver increased by 9.37% when using the cavity receiver instead of the external receiver, due to the reduction of heat loss. For the cavity receiver, both radiative and reflective heat loss occurred inside the receiver aperture, which was much smaller than that of the cylindrical design. The convective loss occurred at the inner surfaces including both the active and passive parts, which had an approximately 44% heat transfer area larger than the cylindrical design. However, air temperature inside the cavity was much higher than the outside temperature, which could effectively reduce the convective heat loss. Based on the temperature difference between the wall and external air, the equivalent convective heat transfer coefficient of the cavity inner surface can be acquired from Eq. (14) and Eq. (20), which was about $8W/m^2 \cdot K$ for the cavity receiver and $14W/m^2 \cdot K$ for the external receiver. The difference can reduce the convective loss of the cavity receiver in further compared to that of cylindrical case. As shown in table 3, it can be found that much smaller heat loss was achieved for the present new design. The calculated global receiver thermal efficiency of the present proposed dual-receiver was 3.2% higher than that of the original two-cylinder setup.

Table 3. The solar field and thermal efficiency under the design conditions for the present dual-receiver and the two-cylinder setup.

		Present dual-receiver	Two-cylinder setup
Solar field efficiency (%)	Boiler	72.37	72.27
	Superheater	71.74	72.51
	Global	72.17	72.33

Receiver efficiency (%)	Boiler	88.16	87.98
	Superheater	82.64	73.27
	Global	86.55	83.35
Superheater heat loss efficiency (%)	Convective loss	4.84	5.4
	Radiative loss	9.52	16.32
	Reflective loss	3	5

Table 4 compares the overall performance of the two dual-receiver designs. Assuming the same generator efficiency, the total solar plant efficiency was improved by 0.76% for the present proposed dual-receiver, correspondingly producing extra 0.3MW electrical power.

Table 4. Overall performance at design conditions for the present dual-receiver and the two-cylinder setup.

	Present dual-receiver	Two-cylinder setup
Solar field performance	69.2MW→50MW	69.2MW→50.1MW
Receiver performance	50MW→43.2MW	50.1MW→41.7MW
Thermal power to storage	10.8MW	10.4MW
Thermal power to turbine	32.4MW	31.3MW
Net Rankine cycle efficiency and electric power	35% 11.3MW	35% 11MW
Overall performance at design conditions	21.86%	21.1%

4.3 Off-design performance of the proposed dual-receiver

To examine the performance of the new design under off-design conditions, different solar time of the spring equinox day was considered, which changed the solar flux map on the receiver and correspondently the inlet mass flow rate of HTF.

Comparing Fig. 9 and Fig. 10, which show respectively the incident surface flux distribution for the present dual-receiver at 8:00am and 10:00am of the spring equinox day, it can be found that the solar flux peaks of both boiling and superheating receivers moved from east to west when time changes from 8:00am to 12:00am, due to the solar azimuth moves. Different to the symmetrical case as in the noon as shown in Fig. 4, there was an unbalalnced distribution of heat fluxes at the off-design times shown in Fig. 9 and 10. For instance, the maximum heat flux of left side receiver was about two times as that of rght side, as shown in Fig. 9(a). Hence, to accommodate the requirement of the same exit quality from the boiler, the mass flow rate should be reduced corresponding to the reduction in the incident surface heat flux, so did the exit steam temperature from the superheater.

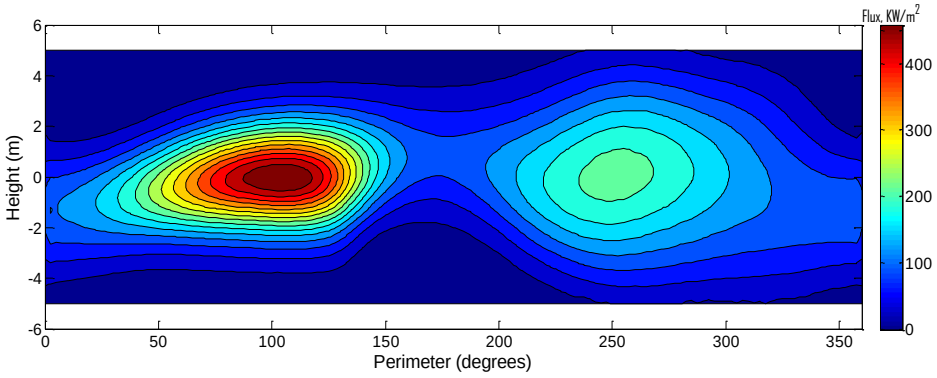

(a) Boiling receiver (Perimeter at 180^o is north direction).

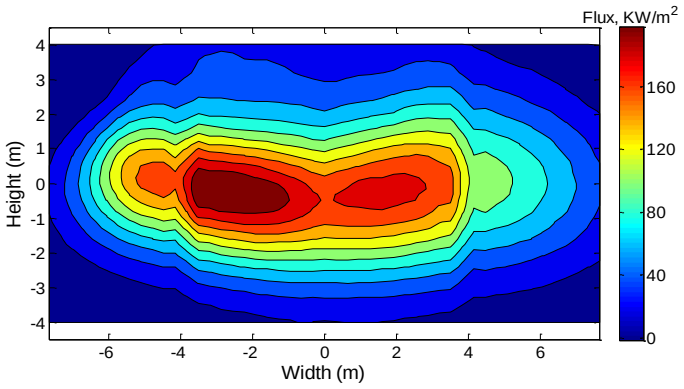

(b) Superheating receiver.

Fig. 9. Surface heat flux distribution for the dual-receiver at 8:00am of the spring equinox day.

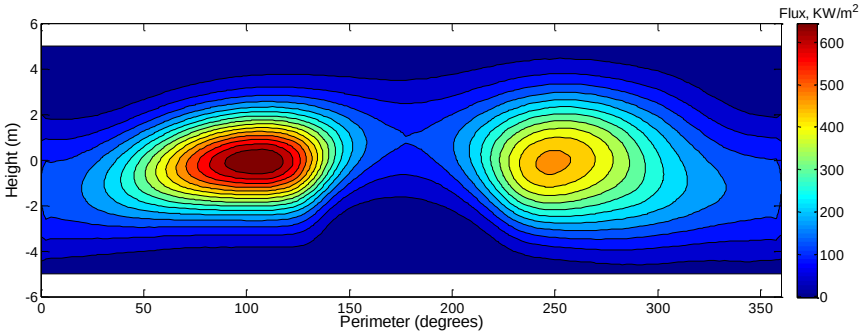

(a) Boiling receiver (Perimeter at 180^{o} is north direction).

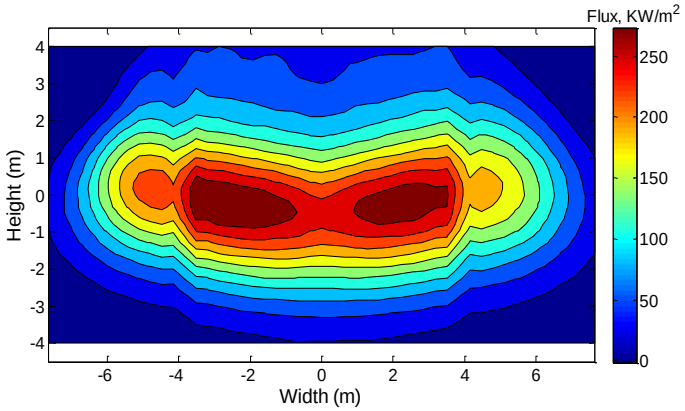

(b) Superheating receiver.

Fig. 10. Surface heat flux distribution for the dual-receiver at 10:00am of the spring equinox day.

Table 5 lists the heat losses and the performance of each parts of the present dual-receiver at 8:00am, 10:00am and 12:00am of the spring equinox day. Due to the decrease in the surface temperature in the morning, both radiation and convective heat losses were reduced. However, the percentages of these heat losses were increased for both boiling and superheating sections, due to the reduction in the total heat input, which was decided by the DNI and solar field efficiency.

Comparing to the boiling section, the radiative heat loss became dominant in the superheating section, which varied from 9.5% to 13.2% at different times, due to its strong dependence on the wall temperature, as indicated by Eq. (12). For the boiling section, the wall temperature was mainly

decided by the saturation temperature of the fluid, which only varied slightly at different off-design points. As a contrast, the increase of the wall temperature in the superheating section can be 200-300K higher than that of the boiling section, which is therefore responsible for the increased heat loss from the radiation.

Similar cases were found at other comparative time points, i.e. 12:00am of the summer solstice day and 9:00am of the winter solstice day, which were chosen to illustrate the thermal efficiency performances of the present new design. It was obtained that the thermal efficiency varied from 80% to 87%. It should be noted that when 9:00am of the winter solstice day, outlet steam temperature was 496^{o}C, which was 19^{o}C lower than the design value of the outlet steam temperature. Such a lower outlet steam temperature would lead to lower Rankine cycle efficiency and higher humidity on the last stages of the steam turbine. As typical allowable outlet steam temperature deviation is from -10 to 5^{o}C [22], the inlet mass flow rate or the number of heliostats corresponding to boiling and superheating receiver shall be adjusted to obtain appropriate outlet steam temperature under such conditions .

Table 5. The present dual-receiver performances at different time points.

Time	spring equinox 12:00am	spring equinox 10:00am	spring equinox 8:00am	summer solstice 12:00 am	winter solstice 9:00am
DNI (W/m^2)	914	869	685	937	573
Solar field efficiency (%)	72.17	69.69	60.85	71.65	58.39
Evaporator specific mass flow rate (kg/m$^{2\cdot}$ s)	540-880	449-807	242-625	566-887	164-538
Superheater outlet flow rate (kg/s)	17.3	15.7	10.4	17.6	8.1
Superheater outlet steam temperature (^{o}C)	515	515	510	515	496
Boiling receiver thermal efficiency (%)	88.16	87.61	84.58	88.26	82.29

Convective loss (%)	2.46	2.67	3.8	2.42	4.67
Radiative loss (%)	4.38	4.72	6.62	4.31	8.05
Reflective loss (%)	5	5	5	5	5
Superheater receiver thermal efficiency (%)	82.64	81.78	77.04	82.82	73.28
Convective loss (%)	4.84	5.12	6.79	4.78	8.33
Radiative loss (%)	9.52	10.1	13.17	9.4	15.39
Reflective loss (%)	3	3	3	3	3
Total Receiver thermal efficiency(%)	86.55	85.89	82.34	86.66%	79.78

4.4 Influence of tube diameter

For a consistent comparison, the influence of tube diameter on the system performance was investigated under the same solar flux map, geometry of receiver, inlet water/steam parameters, inlet total mass flow rate and tube thickness as in section 3.

For the boiling receiver, the mass flow rate in each parallel rising panel was different to ensure that the pressure drop through all panels was equal. When the tube outer diameter was reduced, the mass flow rate was found to increase for the panels with relatively lower surface heat fluxes, but decreased for panels with higher surface heat fluxes. This can be attributed to the different pressure drop components. For low heat flux panels, the gravitational pressure drop was dominant, whereas for higher heat flux panels, the frictional component was the major contribution. Consequently, the higher heat flux panels were prone to the overheating problem due to the reduction in the mass flow rate, which should be considered in practice. One potential solution would be the proper use of throttle orifices, which should be located at the panel entrance with adjustable orifice diameters suitable for different heat fluxes. For the east half of boiling panels, the local resistance coefficients

were set as 115, 94, 60, 25, 0, 17, 86 and 123, respectively from south to north, and the local resistance coefficients remained the same for different tube diameters.

Table 6 shows the influence of tube outer diameter on the boiling receiver. When the tube outer diameter was reduced from 26mm to 16mm, the flow velocity was increased under the same mass flow rate, resulting in the increase of the heat transfer coefficient. The thermal efficiency of the boiling receiver, excluding the parasitic loss, was increased by only ~0.05%. This was, however, compromised by a sharp increase in the pressure drop, i.e., from 85kPa to 772kPa. The overall receiver thermal efficiency was reduced from 87.86% to 85.53% when the increased pumping power was considered. Clearly it is not always beneficial to decrease the tube size, which shall be considered collectively for the boiler section.

Table 6. Influence of tube outer diameter for boiling receiver.

Tube outer diameter (mm)	Boiling receiver thermal efficiency excluding parasitic loss (%)	Flow velocity (m/s)	Heat transfer coefficient ($kW/m^2 \cdot k$)	Pressure drop (kPa)	Boiling receiver thermal efficiency including parasitic loss(%)
26	88.16	0.8-4.3	7.3-46.7	85	87.86
24	88.16	0.9-4.8	8.9-48.8	102	87.81
22	88.16	1.2-5.7	11.4-53.7	136	87.7
20	88.16	1.7-7	14.9-54.8	201	87.49
18	88.17	2.3-9	17.9-59.9	342	87.02
16	88.21	3.5-13	25.3-70.9	772	85.53

For the superheating receiver, the influence of tube outer diameter is shown in Table 7. When the tube outer diameter was reduced from 26mm to 14mm, the receiver thermal efficiency was improved by ~3%, much higher than the boiler section. This is related to the relative importance of different heat resistance. For the boiling section, the main resistance to heat loss was from the wall

and further improve the flow boiling heat transfer coefficient would not change the heat loss. However for the superheating section, the major heat resistance came from the internal convection. A size reduction would reduce the heat loss saliently due to the increased in heat transfer coefficient inside the pipe. However as previously, the pressure drop was also raised significantly from 8kPa to 585kPa. A parametric study of the size effect suggested that the thermal efficiency of the superheating receiver, including parasitic loss, reached its maximum performance at an outer diameter of 18mm.

Table 7. Influence of tube outer diameter for superheating receiver.

Tube outer diameter (mm)	Superheating receiver thermal efficiency excluding parasitic (%)	Flow velocity (m/s)	Heat transfer coefficient ($kW/m^2 \cdot k$)	Pressure drop (kPa)	Superheating receiver thermal efficiency including parasitic loss (%)
26	82.83	3.9-7.4	1-2.4	8	82.68
24	83.36	4.6-8.6	1.5-2.8	13	83.14
22	83.85	5.4-10.2	1.8-3.3	21	83.51
20	84.39	6.7-12.8	2.2-4	39	83.82
18	84.85	8.6-16.5	2.8-5.1	76	83.83
16	85.36	12-23.4	3.8-7	186	83.05
14	85.83	18.6-37.4	5.7-10.4	585	78.17

5 Conclusions

A novel dual-receiver with a surrounding solar field was proposed to improve the efficiency of solar power tower (SPT). The new concept comprised an external receiver and a cavity receiver, respectively designated for the boiling section and superheating section, providing a convenient yet simple approach to control the heat flux distribution on both sections.

(1) The new design of 11MW solar power plant achieved an overall thermal efficiency of 86.55% under design conditions, generating 17.3kg/s superheated steam at 515^{o}C and 10.7MPa.

(2) A comparative study of 11MW solar power plant was conducted based on the new design and a two-external cylindrical setup. The present design improved the thermal efficiency of the superheating section by about 9.37%, and the global thermal efficiency of the SPT by 3.2%.

(3) The plant performance was affected significantly by the incident solar fluxes at different time of a day, and even exceeded the range of allowable outlet steam temperature, which required a proper control of the inlet mass flow rate or the heliostats focus.

(4) It is not always beneficial to decrease the tube size for the benefit of heat transfer enhancement and an optimized tube diameter of ~18 mm for the superheating receiver was proposed based on the collective consideration of the heat transfer effect and pumping power requirement.

Appendix. Model validation

Monte-Carlo method is validated in this section. By using original heliostat field layout of PS10 power plant and receiver data, net power and flux peak of PS10 receiver at the noon of the spring equinox day were obtained by Monte-Carlo method. Table A1 gives the comparison of PS10 data [13] and our Monte-Carlo method simulated results. It can be seen that Monte-Carlo method is very close to literature data, and the method was then used in this study to configruate the heliostat fields.

Table A1. Comparison of net power and flux peak between data of PS10 and the present Monte-Carlo results at noon of the spring equinox day.

	PS10 literature data	Monte-Carlo
Net power (MW)	51.9	51.5
Flux peak (kW/m^2)	644	650

Acknowledgment

The financial supports for this research project from the National Natural Science Foundation of China (No.U1361108), the national "973 Program" of China (No. 2015CB251503) and the 111 Project (B12034) are gratefully acknowledged.

References

[1] O. Behar, A. Khellaf, K. Mohammedi, A review of studies on central receiver solar thermal power plants, Renewable and Sustainable Energy Reviews, 23 (2013) 12-39.

[2] A.L. Avila-Marin, J. Fernandez-Reche, F.M. Tellez, Evaluation of the potential of central receiver solar power plants: Configuration, optimization and trends, Applied Energy, 112 (2013) 274-288.

[3] L. Yebra, M. Berenguel, S. Dormido, M. Romero, Modelling and simulation of central receiver solar thermal power plants, in: Decision and Control, 2005 and 2005 European Control Conference. CDC-ECC'05. 44th IEEE Conference on, IEEE, 2005, pp. 7410-7415.

[4] R. Osuna, V. Fernandez, M. Romero, M.J. Marcos, PS10, A 10 MW Solar Tower Power Plant for Southern Spain, in, 2001.

[5] J.E. Pacheco, eSolar's Modular Concentrating Solar Power Tower Plant and Construction of the Sierra Solar Generating Station, in: ASME 2009 3rd International Conference on Energy Sustainability collocated with the Heat Transfer and InterPACK09 Conferences, American Society of Mechanical Engineers, 2009, pp. 701-705.

[6] E. Xu, Q. Yu, Z. Wang, C. Yang, Modeling and simulation of 1 MW DAHAN solar thermal power tower plant, Renewable Energy, 36 (2011) 848-857.

[7] T.M. Pavlović, I.S. Radonjić, D.D. Milosavljević, L.S. Pantić, A review of concentrating solar power plants in the world and their potential use in Serbia, Renewable and Sustainable Energy Reviews, 16 (2012) 3891-3902.

[8] L. Crespo, F. Ramos, F. Martínez, Questions and answers on solar central receiver plant design by NSPOC, in: 17th annual SolarPACES symposium, 2011.

[9] J. Sanz-Bermejo, V. Gallardo-Natividad, J. Gonzalez-Aguilar, M. Romero, Comparative System Performance Analysis of Direct Steam Generation Central Receiver Solar Thermal Power Plants in Megawatt Range, Journal of Solar Energy Engineering, 136 (2014) 011028.

[10] Y. Gilon, I. Kroizer, G. Kroyzer, Method and control system for operating a solar power tower system, U.S. Patent No. 8,001,960, (2011).

[11] M.S. Gonzalez, R.O. Gonzalez-Aguilar, V.F. Quero, R.N. Gilaberte, Solar concentration plant for the production of superheated steam, U.S. Patent No. 8,365,720, (2013).

[12] R. Ben-Zvi, M. Epstein, A. Segal, Simulation of an integrated steam generator for solar tower, Solar Energy, 86 (2012) 578-592.

[13] V.D. Fernández, PS10: a 11.0-MWe Solar Tower Power Plant with Saturated Steam Receiver, (2005). <http://www.upcomillas.es/catedras/crm/report05/Comunicaciones/Mesa%20IV/D%20Valerio%20Fern%C3%A1ndez%20-%20Solucar%202.pdf>.

[14] F.J. Collado, J. Guallar, A review of optimized design layouts for solar power tower plants with campo code, Renewable and Sustainable Energy Reviews, 20 (2013) 142-154.

[15] J. Zambrana, T.J. Leo, P. Perez-del-Notario, Vertical tube length calculation based on available heat transfer coefficient expressions for the subcooled flow boiling region, Applied Thermal Engineering, 28 (2008) 499-513.

[16] L. Zhonghu, Two-phase of steam and water and heat transfer, Xian Jiaotong University Press, 1987.

[17] V. Prodanovic, D. Fraser, M. Salcudean, On the transition from partial to fully developed subcooled flow boiling, International journal of heat and mass transfer, 45 (2002) 4727-4738.

[18] D.L. Siebers, J.S. Kraabel, Estimating convective energy losses from solar central receivers, in, Sandia National Labs., Livermore, CA (USA), 1984.

[19] M. Montiel Gonzalez, J. Hinojosa Palafox, C.A. Estrada, Numerical study of heat transfer by natural convection and surface thermal radiation in an open cavity receiver, Solar Energy, 86 (2012) 1118-1128.

[20] N. Lauzier, View Factors with GUI, (2004). <http://www.mathworks.com/matlabcentral/fileexchange/5664-view-factors>.

[21] L. Jianming, Solar thermal power generation technology, Chemical Industry Press, 2012.

[22] GB/T 753-2012 Steam condition series for utility boiler, (2012).

Table captions

Table 1. Main parameters used in the optical analysis.

Table 2. Geometry designs and thermodynamic parameters of the present dual-receiver and the two-cylinder setup.

Table 3. The solar field and thermal efficiency under the design conditions for the present dual-receiver and the two-cylinder setup.

Table 4. Overall performance at design conditions for the present dual-receiver and the two-cylinder setup.

Table 5. The present dual-receiver performances at different time points.

Table 6. Influence of tube outer diameter for boiling receiver.

Table 7. Influence of tube outer diameter for superheating receiver.

Table A1. Comparison of net power and flux peak between data of PS10 and the present Monte-Carlo results at noon of the spring equinox day.

Figure captions

Fig. 1. Schematic diagram of the proposed dual-receiver with solar field.

Fig. 2. Heliostat field layout of the proposed dual-receiver.

Fig. 3. The bottom cavity receiver. (a) The cavity receiver geometry. (b) Fluid flow layout of the active heated walls.

Fig. 4. Surface heat flux distribution for the dual-receiver at the noon of the spring equinox day. (a) Boiling receiver (Perimeter of180º is north direction). (b) Superheating receiver.

Fig. 5. Panel surface temperature distribution of the top boiling receiver (Perimeter of 0m is the north direction).

Fig. 6. Panels surface temperature distribution of the bottom superheating receiver.

Fig. 7. Schematic diagram of the two-cylinder setup with surrounding heliostat field.

Fig. 8. Heliostat field layout of the two-cylinder setup.

Fig. 9. Surface heat flux distribution for the dual-receiver at 8:00am of the spring equinox day. (a) Boiling receiver (Perimeter at 180o is north direction). (b) Superheating receiver.

Fig. 10. Surface heat flux distribution for the dual-receiver at 10:00am of the spring equinox day. (a) Boiling receiver (Perimeter at 180o is north direction). (b) Superheating receiver.